SCIENTIFIC REPORTS
nature research

OPEN

Probing the structure and electronic properties of beryllium doped boron clusters: A planar BeB_{16}^- cluster motif for metallo-borophene

Received: 7 June 2019
Accepted: 16 September 2019
Published online: 07 October 2019

Dongliang Kang[1], Weiguo Sun[1], Hongxiao Shi[1], Cheng Lu[2], Xiaoyu Kuang[1], Bole Chen[1], Xinxin Xia[1] & George Maroulis[3]

Beryllium-doped boron clusters display essential similarities to borophene (boron sheet) with a molecular structure characterized by remarkable properties, such as anisotropy, metallicity and high conductivity. Here we have determined low-energy structures of $BeB_n^{0/-}$ ($n = 10$–20) clusters by utilizing CALYPSO searching program and DFT optimization. The results indicated that most ground states of clusters prefer plane or quasi-plane structures by doped Be atom. A novel unexpected fascinating planar BeB_{16}^- cluster with C_{2v} symmetry is uncovered which possesses robust relative stability. Furthermore, planar BeB_{16}^- offers a possibility to construct metallo-borophene nano-materials. Molecular orbital and chemical bonding analysis reveal the peculiarities of BeB_{16}^- cluster brings forth the aromaticity and the strong interaction of B-B σ-bonds in boron network.

Molecular geometric configuration and attributes of pure[1–3] and doped boron clusters[4–9] have drawn much attention in recent years. The use of boron clusters as subunits in novel bioactive architectures with potential use as drugs is of primary importance[10]. From a Materials Science perspective the emergence of graphene[11] and synthetic two-dimensional structures as silicene[12,13], germanene[14], stanene[15], antimonene[16], bismuthene[17,18] and tellurene[19] have opened new pathways for modern research[20–22]. Relying on experimental and theoretical work, Hersam's group[23] have confirmed and established the synthesis of 2D boron polymorphs (borophene) characterized by anisotropy and metallicity, and paved the way to investigations leading to the discovery of novel materials. Recently, it was reported that magnesium diboride (MgB_2), which consists of graphene-like honeycomb networks of sandwiched boron, shows superconductivity[24]. It should be noted that beryllium has the same valence electrons number with magnesium. Be-doped boron clusters appear to have significant potential candidate as layered 2D materials[25–28]. This certainly gives reason for more systematic investigations.

Boron is the lightest metalloid chemical element, the lowest-Z element[23] with a trivalent outer shell[29,30]. Consequently, boron does not form closed-shell electronic structures via conventional covalent bonds[31–33], but favors delocalized chemical bonds with electron pairs shared among three (or more) atoms instead. Recently, systematic investigations of pure boron clusters in term of the anisotropy and polymorphism have brought forth new significant findings leading to the design of new borides. A selection of characteristic architectures of pure boron clusters includes: tank tread[34], wankel motor[35–39], wheel-like[40], boron nanotubes[41], B_{12} icosahedra[42], buckyballs[43], fullerene[44], B_{36} with hexagonal holes (HHs)[45], naphthalene[46], borospherene[47] and more. Co and Rh doped B_{12}^- clusters featured half-sandwich structure has been reported by Wang and co-workers[48]. There followed the Co-centered boron molecular drums structure for the CoB_{16}^- cluster[49]. Additional work by the same group includes the Mn-centered tubular boron cluster for MnB_{16}^-, a drum and quasi-planar structure for RhB_{18}^- and the planar CoB_{18}^-[50–52]. Very recently, Cui and co-workers reported tubular structures for LiB_{20} and LiB_{20}^-[53]. These

[1]Institute of Atomic and Molecular Physics, Sichuan University, Chengdu, 610065, China. [2]School of Mathematics and Physics, China University of Geosciences (Wuhan), Wuhan, 430074, China. [3]Department of Chemistry, University of Patras, GR-26500, Patras, Greece. Correspondence and requests for materials should be addressed to X.K. (email: scu_kuang@163.com) or G.M. (email: maroulis@upatras.gr)

impressive findings reveal that single metal atom doping leads to new opportunities for the use of boron clusters as geometrical ligands.

Several theoretical investigations of boron clusters with doping transition-element serve as the object of discovering new materials recently[54,55]. The alkaline-earth metal-doped boron clusters and Be-doped ones in particular have been systematically studied[56–58]. Nevertheless, more systematic work is needed to systematize and deepen our understanding of Be-doped boron clusters. To fill the existing lacunae and bring forth new insights on medium-sized Be-doped boron clusters, we have thoroughly investigated $BeB_n^{0/-}$ clusters.

Results and Discussion

Geometric configurations and photoelectron spectra. The determined low-energy $BeB_n^{0/-}$ ($n = 10$–20) are showed in Figs 1 and 2. We labeled each isomer using nt/t$^-$ (t = a, b, c), therein nt stands for the neutral clusters and nt$^-$ stands for the anionic clusters. The lowest-energy structures $BeB_n^{0/-}$ ($n = 10$, 12, 13, 14, 15, 16) and BeB_{11}^- are quasi-planar structures. The lowest-energy structure BeB_{11} shows a half-sandwich structure consisting of one half-sandwich structure composed by eleven boron atoms and one Be atom in the center. The lowest-energy structures $BeB_{17}^{0/-}$ like a trapezoid and its center portion appear on the convex. The lowest-energy structure of BeB_{18} and BeB_{20}^- are 3D cage-like structure. The lowest-energy structure BeB_{18}^- with a parallelogram located in the center displays a planar structure. The ground-state structures $BeB_{19}^{0/-}$ and BeB_{20} can be viewed as plate-like structures (in Figs S4 and S5 of Supplementary Information). The lowest-energy structures of $BeB_n^{0/-}$ clusters are generally evolutional from the quasi-planar to 3D cage-like or plate-like structures. For plane and quasi-planar structures, the coordinate number of Be atom is interesting. The $BeB_n^{0/-}$ ($n = 10$, 12, 14, 16) and BeB_{18}^- feature heptacoordinate and the BeB_{11}^- and $BeB_n^{0/-}$ ($n = 13$, 15) possess octacoordinate, while the $BeB_{17}^{0/-}$ are quasi-planar hexacoordinate structures due to the attribute of Be atom[59,60]. This evident structures evolution pattern contributes to form plane clusters of $BeB_n^{0/-}$, which are potential two-dimensional material. The metastable of nb/b$^-$ ($n = 10$–13) clusters display half-sandwich architectural feature, while when the cluster sizes increase $n \geq 14$, the clusters are varies cage-like, quasi-planar and plate-like structures. The nc/c$^-$ ($n = 10$–18) clusters display half-sandwich, plane, cage-like structures, different from the larger size isomers ($n \geq 19$) are double-ring and plate-like structures.

To get a deep understand to differences between different metal-doped clusters, we provide a comparison for doped boron clusters. The transition-metal doped boron clusters, NbB_{10}^- and TaB_{10}^-, are wheels structures with high coordination number[4], while $BeB_{10}^{0/-}$ clusters are quasi-planar structures with one B-Be unit inside. For doped B_{12} clusters, the prior works report that half-sandwich structures VB_{10}^-, CoB_{12}^- and RhB_{12}^- clusters[4,48] are different with $BeB_{12}^{0/-}$ clusters, which are standard quasi-planar structures featuring a triangle in the center. Compare with drum-like CoB_{16}^- cluster[49] and tubular-like MnB_{16}^- cluster[50], the ground state $BeB_{16}^{0/-}$ display quasi-plane structures. It is worth noting that adjacent alkali element Lithium doped into B_{20} display highly symmetrical tubular $LiB_{20}^{0/-}$ clusters[53]. We report BeB_{20} and BeB_{20}^- are plate-like and 3D cage-like structures, respectively. The reason for the structural differences of same-sized clusters may be doped-metals have different valence electron and atomic radius[61].

Photoelectron spectra (PES) analysis, obtained via a TD–DFT approach, is of absolute importance for the assessment of the nature of the determined lowest-energy structures. We simulated the PES of BeB_n^- clusters and the results are displayed in Fig. 3. Our group also simulated the PES of some other cluster system using the method[62,63]. The PES pattern of the BeB_{10}^- possesses five peaks located at 3.26, 3.75, 4.18, 4.75 and 5.77 eV. The PES of BeB_{11}^- possesses four clear peaks at 3.45, 4.21, 4.59, and 5.01 eV, with B and C peaks forming a broad bond. For BeB_{12}^-, we observe three major peaks at 2.90, 4.21 and 4.50 eV, wherein the double-peak feature (A and B) is prominent and broad. The BeB_{13}^- PES contains five major peaks at 3.16, 3.49, 4.32, 4.75 and 5.22 eV. The relevant broad bond is found at triple-peak feature consisted of peaks B, C and D. Five peaks are observed for BeB_{14}^- at 3.33, 3.86, 4.16, 4.63 and 5.45 eV. The peaks A, B and C constitute a relatively wide bond. For BeB_{15}^- there are five major peaks at 3.46, 4.28, 4.64, 5.06 and 5.82 eV, whereas the BeB_{16}^- spectrum has only two sparse peaks at 4.08 and 5.25 eV. The well-structure spectrum of BeB_{17}^- shows five peaks at 3.90, 4.32, 4.79, 5.13 and 5.49 eV, suggesting a greater span triple-peak feature (B, C and D). A crowded spectrum pattern BeB_{18}^- has five peaks observed at 3.59, 3.98, 4.21, 5.13 and 5.57 eV, with two broad bonds. There are five peaks in the spectrum of BeB_{19}^- at 3.63, 4.73, 5.13, 5.51 and 5.82 eV, therein an unfitted bond is located at the range between 4.5 to 6.0 eV. The spectrum of BeB_{20}^- possesses five peaks at 2.59, 3.36, 4.43, 4.85 and 5.79 eV.

Relative stabilities. We characterize the inherent stability of the $BeB_n^{0/-}$ ($n = 10$–20) clusters by computing the E_b (eV), according to the following formula:

$$E_b(BeB_n) = [nE(B) + E(Be) - E(BeB_n)]/(n+1) \quad (1)$$

$$E_b(BeB_n^-) = [(n-1)E(B) + E(B^-) + E(Be) - E(BeB_n^-)]/(n+1) \quad (2)$$

The average binding energy (E_b) of a cluster is clearly a measure of its thermodynamic stability. An increase in E_b means a higher stability. The value of neutral BeB_n clusters less than the value of their anionic counterparts in Fig. S1(a), indicating that the anionic clusters feature higher thermodynamically. The trend of the curves for both neutral and anionic are gradually upward indicated that the high thermodynamic stability with the cluster size increases. The second vital physical quantity we take into account here is the $\Delta^2 E$. The relevant formulae are

$$\Delta^2 E(BeB_n) = E(BeB_{n-1}) + E(BeB_{n+1}) - 2E(BeB_n) \quad (3)$$

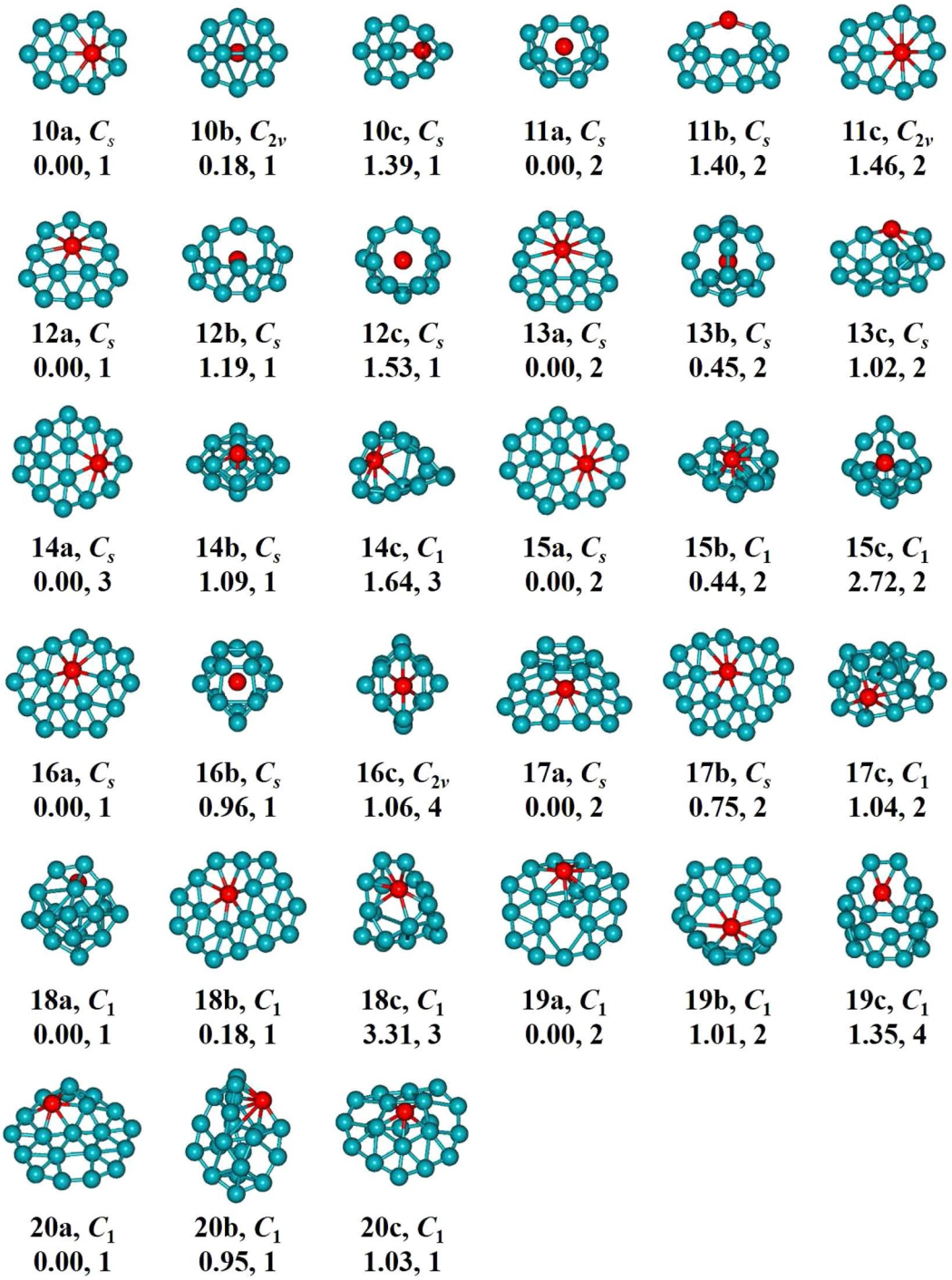

Figure 1. Low-lying geometrical structures of BeB_n ($n = 10$–20) clusters. "a" stands for the lowest-energy structures. "b" and "c" stand for the metastable state structures.

$$\Delta^2 E(BeB_n^-) = E(BeB_{n-1}^-) + E(BeB_{n+1}^-) - 2E(BeB_n^-) \quad (4)$$

As inferred from Fig. S1(b), both of the neutral and anionic curves show odd-even alteration. The evident peak values generated at $n =$ even number, suggest that clusters with the even boron atoms feature higher stability than which with odd boron atoms. Finally, we discuss the HOMO-LUMO energy gap (E_{gap}) which provides a valuable index of the stability of clusters. Large values indicate strong chemical stability. We summarize the E_{gap} values of the lowest-energy $BeB_n^{0/-}$ clusters in Table 1, and the line chart is displayed in Fig. S1(c). From the latter we can clearly see some apparent local maxima: BeB_{11} and BeB_{16}^-, which means that they feature higher stability

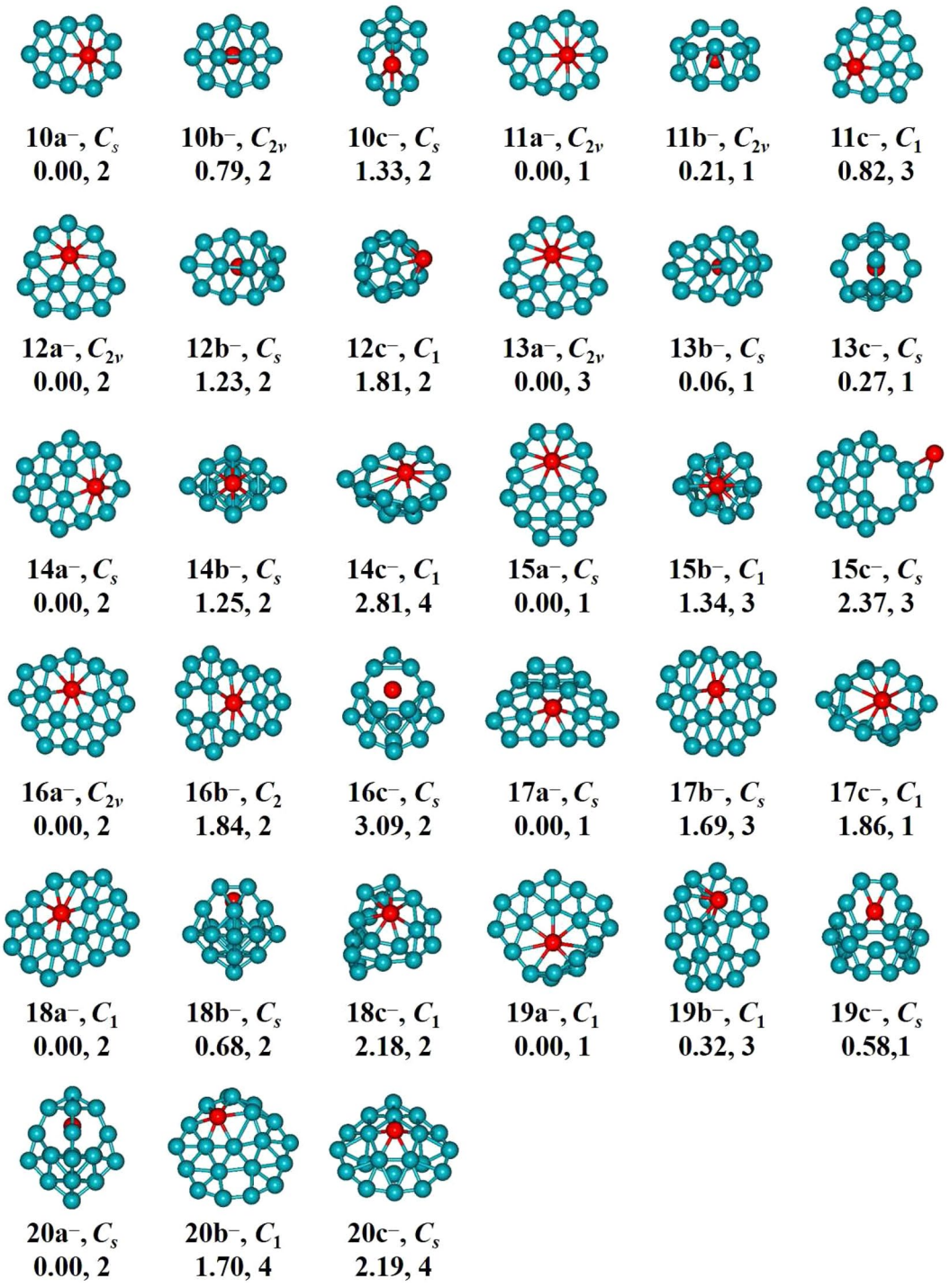

Figure 2. Low- lying geometrical structures of BeB_n^- ($n = 10$–20) clusters. "a" stands for the lowest-energy structures. "b" and "c" stand for the metastable state structures.

than the others. Consequently, based on the above analyses, we can reach a definitive conclusion that the BeB_{16}^- can seen as a "magic" cluster.

Chemical banding. To deeply perceive the bonding nature of BeB_{16}^- (C_{2v} symmetry), we display eleven MO figures for BeB_{16}^-, including one LUMO, one HOMO and nine HOMO-n ($n = 1$–9) in Fig. 4 by analyzing the chemical bonding. The LUMO, HOMO, HOMO-2, HOMO-5 and HOMO-9 dominated primarily by π_p and π_p^* orbitals are a direct interaction 2p orbitals of B atoms. The HOMO-n ($n = 1, 4, 8$) feature σ_p and σ_p^* orbitals. The HOMO-n ($n = 3, 6, 7$) features σ_p, σ_p^*, σ_{sp} and σ_{sp}^* orbitals. AdNDP analysis distributes 51 valence electrons into different regions as reflected by the occupation numbers (ONs) in Fig. 5. We divide it into three sets. The first set consists of twelve 2c-2e (1.79–1.93 |e|) localized σ-bonds. The second set consists of nine delocalized σ-bonds,

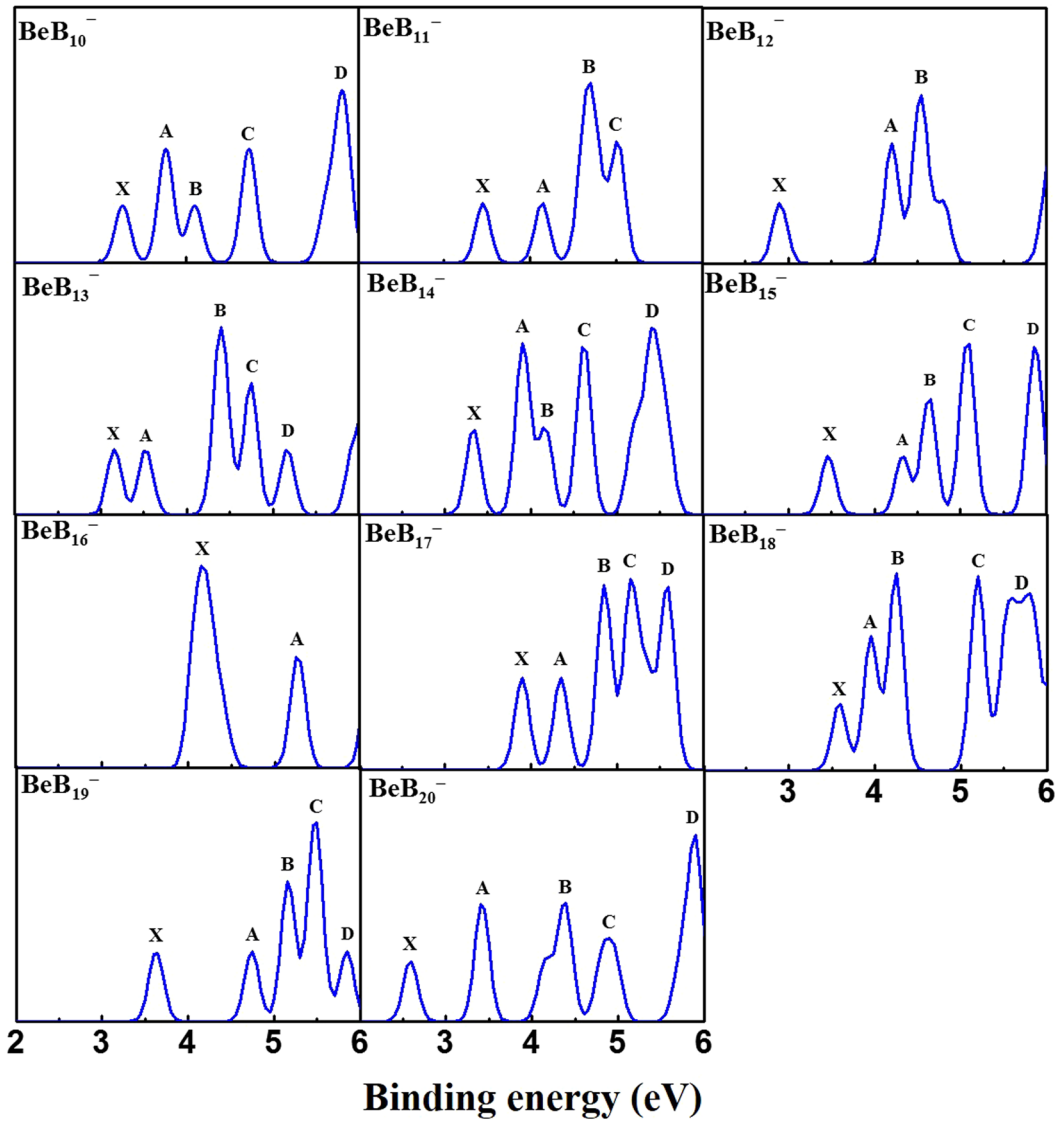

Figure 3. The simulated PES of BeB_n^- ($n = 10–20$) clusters.

BeB_n					BeB_n^-			
n	Sta.	Sym.	E_b	E_{gap}	Sta.	Sym.	E_b	E_{gap}
10	$^1A'$	C_s	4.69	2.93	$^2A''$	C_s	5.06	2.81
11	$^2A'$	C_s	4.73	3.30	$^1A_1$	C_{2v}	5.08	2.36
12	$^1A'$	C_s	4.87	2.94	$^2A_2$	C_{2v}	5.17	1.66
13	$^2A''$	C_s	4.84	1.74	$^3B_2$	C_{2v}	5.14	2.17
14	$^3A''$	C_s	4.90	2.47	$^2A''$	C_s	5.23	2.14
15	$^2A''$	C_s	4.93	1.85	$^1A'$	C_s	5.20	1.89
16	$^1A'$	C_s	4.99	1.77	$^2B_2$	C_{2v}	5.29	2.93
17	$^2A'$	C_s	5.03	2.17	$^1A'$	C_s	5.30	2.03
18	^1A	C_1	5.08	2.60	^2A	C_1	5.32	1.89
19	^2A	C_1	5.18	1.97	^1A	C_1	5.25	2.39
20	^1A	C_1	5.10	2.67	$^2A'$	C_s	5.31	2.09

Table 1. The calculated electronic states, symmetries, average binding energies (E_b, in eV) and energy gaps (E_{gap}, in eV) of $BeB_n^{0/-}$ clusters in the size range of $n = 10–20$.

which are five 3c-2e (1.79–1.86 |e|), two 4c-2e (1.72 |e|), and two 4c-2e (1.79 |e|). The five delocalized π-bonds in last set involving two 4c-2e (1.81 |e|), two 4c-2e (1.83 |e|) and one 17c-2e (2.00 |e|). It is worth nothing that the ON of the 17c-2e π-bonds maintain ON of 2.00 |e|. All values of the ONs listed above ranging from 1.72–2.00 |e|

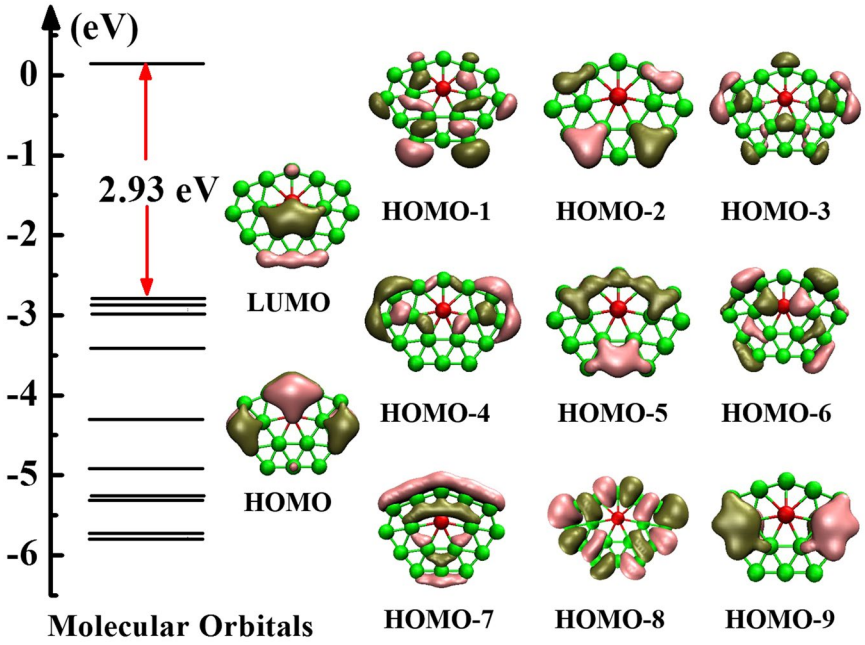

Figure 4. Molecular orbitals for BeB_{16}^- cluster corresponding to different energy level.

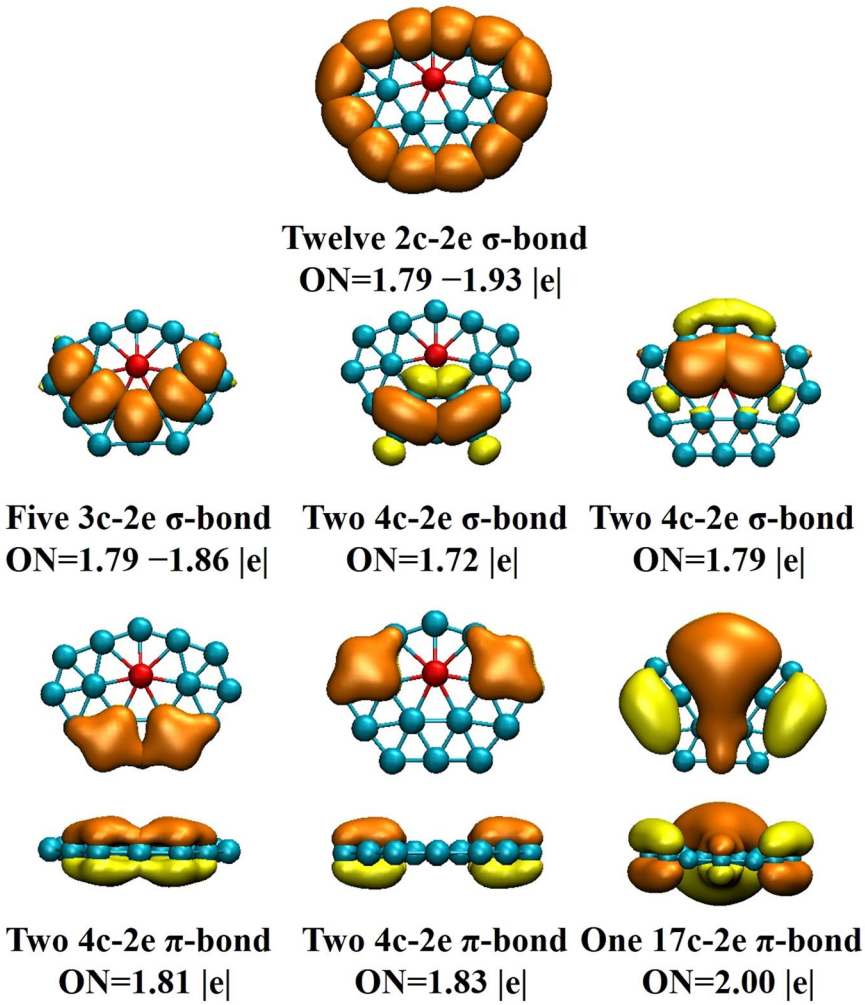

Figure 5. AdNDP analysis of BeB_{16}^- cluster.

are approaching the ideal value 2.00 |e|, which means that the results we calculate is fairly credible. Furthermore, the ten π electrons conform to the $4n+2$ rule ($n=2$), indicating the BeB_{16}^- cluster possesses π-aromaticity, which result to the robust relative stability for BeB_{16}^- cluster.

The Wiberg bond index of BeB_{16}^-, showed in Fig. S2(a), indicate that the bond orders values of B-B (0.13–0.35) greater than the Be-B (0.06–0.11). For Fig. S2(b), the B-B bond lengths (1.54–1.80 Å) are shorter than Be-B bond lengths (1.85–2.03 Å). The results of bond orders and bond lengths show that the peripheral B-B bonds are stronger than the inner Be-B bonds. We have also performed the NPA (natural charge of atom) calculations of $BeB_n^{0/-}$ in Fig. S3 indicate that electron transfer from Be atom to boron fragment. The NPA data of $BeB_n^{0/-}$ ($n=10$–20) clusters are summarized in Table S1. From what has been discussed, we come to the conclusion that the B-B σ-bonds and the aromaticity decide the high stability of BeB_{16}^- cluster. It is worth noting that due to planar structure and chemical bonding characteristics of BeB_{16}^- cluster, also inspired by fascinating prospect of two-dimensional monolayer metallo-borophene[4], we successfully build a schematic of possibility of metallo-borophene (not optimized) based on BeB_{16}^- unit cluster presented in Fig. S6 of Supplementary Information, which indicated the BeB_{16}^- cluster is a potential motif for metallo-borophene.

Conclusions

In summary, the ground-state $BeB_n^{0/-}$ ($n=10$–20) structure obey the evolution rule: quasi-planar to 3D cage-like or plate-like structures, which the doped Be atom contributed to the plane or quasi-plane structures. We hope that the simulated PES can provide valuable guidance for future research on BeB_n clusters and borophene. Based on the relative stability analysis, the BeB_{16}^- cluster characterized by enhanced stability is clearly a "magic" cluster. Chemical bonding analysis indicated that BeB_{16}^- cluster adapt π-aromaticity and the strong interaction of B-B σ-bonds which is deemed as the dominant reasons for the inherent stability of BeB_{16}^- cluster. The planar BeB_{16}^- cluster may serve as a motif for the design of a new boron-based functional material to complement the metallo-borophene effort for synthetic 2D materials development. Our present findings on Be-doped boron clusters should provide valuable information for further explorations of novel cluster architectures.

Computational Methods

We used the CALYPSO code to search the $BeB_n^{0/-}$ ($n=10$–20) clusters. The global explorations of Be-doped boron cluster system was implemented by utilizing particle swarm optimization (PSO) algorithm[64–66]. The effectiveness of this structural prediction method, has been successfully tested on the identification of ground-state structures of various systems[67–69]. To ensure high efficiency in structure predicting, we proceeded to 50 generations for each size, where each generation contains 30 structures. PSO algorithm produces sixty percent of the structures and the rest is generated randomly. The top fifty low-lying isomers were reoptimized with PBE0[70] functional and 6–311 + G(d)[71], as performed via Gaussian 09 package[72]. The PES of Be-doped boron clusters was simulated utilizing TD-DFT method[73]. We then analyzed chemical bonding of BeB_{16}^- cluster relying on the NBO and AdNDP methods[74] at the PBE0/6-311 + G(d) level to display valuable insights into the nature of the bonding by using Multiwfn[75]. The bond orders, bond lengths and NPA are also computed by using the same basis set and method.

References

1. Pham, H. T., Muya, J. T., Buendia, F., Ceulemans, A. & Nguyen, M. T. Formation of the quasi-planar B_{50} boron cluster: topological path from B_{10} and disk aromaticity. *Phys. Chem. Chem. Phys.* **21**, 7039 (2019).
2. Chen, Q. *et al*. Planar B_{38}^- and B_{37}^- clusters with a double-hexagonal vacancy: molecular motifs for borophenes. *Nanoscale*. **9**, 4550–4557 (2017).
3. Arasaki, Y. & Takatsuka, K. Chemical bonding and nonadiabatic electron wavepacket dynamics in densely quasi-degenerate excited electronic state manifold of boron clusters. *J. Chem. Phys.* **150**, 114101 (2019).
4. Li, W. L. *et al*. planar boron clusters to borophenes and metalloborophenes. *Nat. Rev. Chem.* **1**, 0071 (2017).
5. Li, P. F., Du, X. D., Wang, J. J., Lu, C. & Chen, H. H. Probing the Structural Evolution and Stabilities of Medium-Sized $MoB_n^{0/-}$ Clusters. *J. Phys. Chem. C* **122**, 20000–20005 (2018).
6. Li, W. L. *et al*. Recent Progress on the investigations of boron clusters and boron-based materials (I): borophene. *Sci. Sin. Chim.* **48**, 98–107 (2018).
7. Jian, T. *et al*. Probing the structures and bonding of size-selected boron and doped-boron clusters. *Chem. Soc. Rev.* **48**, 3550 (2019).
8. Li, W. L. *et al*. Observation of highly stable and symmetric lanthanide octa-boron inverse sandwich complexes. *Proc. Natl. Acad. Sci. USA* **115**, 30 (2018).
9. Chen, T. T., Li, W. L., Chen, W. J., Li, J. & Wang, L. S. $La_3B_{14}^-$: an inverse triple-decker lanthanide boron cluster. *Chem. Commun.* **55**, 7864 (2019).
10. Hawthorne, M. F. & Maderna, A. Applications of Radiolabeled Boron Clusters to the Diagnosis and Treatment of Cancer. *Chem. Rev.* **99**, 3421–3434 (1999).
11. Geim, A. K. & Novoselov, K. S. Photoelectron Spectroscopy and Ab Initio Study of B_3^- and B_4^- Anions and Their Neutrals. *Nat. Mater.* **6**, 183–191 (2007).
12. Vogt, P. *et al*. Silicene: Compelling Experimental Evidence for Graphenelike Two-Dimensional Silicon. *Phys. Rev. Lett.* **108**, 155501 (2012).
13. Cahangirov, S. *et al*. Electronic Structure of Silicene on Ag(111): Strong Hybridization Effects. *Phys. Rev. B* **88**, 035432 (2013).
14. Davila, M. E., Xian, L., Cahangirov, S., Rubio, A. & Lay, G. L. Germanene: A Novel Two-Dimensional Germanium Allotrope Akin to Graphene and Silicene. *New J. Phys.* **16**, 095002 (2014).
15. Zhu, F. F. *et al*. Epitaxial Growth of Two-Dimensional Stanene. *Nat. Mater.* **14**, 1020–1025 (2015).
16. Ji, J. P. *et al*. Two-Dimensional Antimonene Single Crystals Grown by Van Der Waals Epitaxy. *Nat. Commun.* **7**, 13352 (2016).
17. Nagao, T. *et al*. Nanofilm Allotrope and Phase Transformation of Ultrathin Bi Film on Si(111)–7 × 7. *Phys. Rev. Lett.* **93**, 105501 (2004).
18. Reis, F. *et al*. Bismuthene on a SiC Substrate: A Candidate for a High-Temperature Quantum Spin Hall Material. *Science* **357**, 287–290 (2017).
19. Zhu, Z. L. *et al*. Multivalency-Driven Formation of Te-Based Monolayer Materials: A Combined First Principles and Experimental Study. *Phys. Rev. Lett.* **119**, 106101 (2017).
20. Yu, X. H., Zhang, X. M. & Yan, X. W. Stability of the $Fe_{12}O_{12}$ cluster. *Nano. Res.* **11**, 3574–3581 (2008).

21. Wang, Q. H., Kalantar-Zadeh, K., Kis, A., Coleman, J. N. & Strano, M. S. Electronics and Optoelectronics of Two-Dimensional Transition Metal Dichalcogenides. *Nat. Nanotechnol.* **7**, 699–712 (2012).
22. Ling, X., Wang, H., Huang, S. X., Xia, F. N. & Dresselhaus, M. S. The Renaissance of Black Phosphorus. *Proc. Natl. Acad. Sci. USA* **112**, 4523–4530 (2015).
23. Mannix, A. J., Zhang, Z. H., Guisinger, N. P., Yakobson, B. I. & Hersam, M. C. Borophene as a Prototype for Synthetic 2D Materials Development. *Nat. Nanotechnol.* **13**, 444–450 (2018).
24. Nagamatsu, J., Nakagawa, N., Muranaka, T., Zenitani, Y. & Akimitsu, J. Superconductivity at 39 K in Magnesium Diboride. *Nature* **410**, 63–64 (2001).
25. Li, Q. S. & Jin, Q. Theoretical Study on the Aromaticity of the Pyramidal MB_6 (M = Be, Mg, Ca, and Sr) Clusters. *J. Phys. Chem. A* **107**, 7869–7873 (2013).
26. Adamska, L., Sadasivam, S., Foley, J. J., Darancet, P. & Sharifzadeh, S. First-Principles Investigation of Borophene as a Monolayer Transparent Conductor. *J. Phys. Chem. C* **122**, 4037–4045 (2018).
27. Er, S., Wijs, G. A. & Brocks, G. DFT Study of Planar Boron Sheets: A New Template for Hydrogen Storage. *J. Phys. Chem. C* **113**, 18962–18967 (2009).
28. Jiang, H. R., Lu, Z. H., Wu, M. C., Ciucci, F. & Zhao, T. S. Borophene: A Promising Anode Material Offering High Specific Capacity and High Rate Capability for Lithium-Ion Batteries. *Nano Energy* **23**, 97–104 (2016).
29. Albert, B. & Hillebrecht, H. Boron: Elementary Challenge for Experimenters and Theoreticians. *Angew. Chem. Int. Ed.* **48**, 8640–8668 (2009).
30. Pelaz, L. *et al*. B Diffusion and Clustering in Ion Implanted Si: The Role of B Cluster Precursors. *Appl. Phys. Lett.* **70**, 2285–2287 (1997).
31. Qgitsu, T., Schwegler, E. & Galli, G. β-Rhombohedral Boron: At the Crossroads of the Chemistry of Boron and the Physics of Frustration. *Chem. Rev.* **113**, 3425–3449 (2013).
32. Sergeeva, A. P. *et al*. Understanding Boron through Size-Selected Clusters: Structure, Chemical Bonding, and Fluxionality. *Acc. Chem. Res.* **47**, 1349–1358 (2014).
33. Oganov, A. R. *et al*. Ionic High Pressure form of Elemental Boron. *Phys. Rev. Lett.* **457**, 863–867 (2009).
34. Wang, Y. J. *et al*. Chemical Bonding and Dynamic Fluxionality of a B_{15}^+ Cluster: a Nanoscale Double-Axle Tank Tread. *Phys. Chem. Chem. Phys.* **18**, 15774–15782 (2016).
35. Guajardo, G. M. *et al*. Unravelling Phenomenon of Internal Rotation in B_{13}^+ through Chemical Bonding Analysis. *Chem. Commun.* **47**, 6242–6244 (2011).
36. Jimènez-Halla, J. O. C., Islas, R., Heine, T. & Merino, G. B_{19}^-: An Aromatic Wankel Motor. *Angew. Chem. Int. Ed.* **49**, 5668–5671 (2010).
37. Morene, D. *et al*. B_{18}^{2-}: A Quasi-Planar Bowl Member of the Wankel Motor Family. *Chem. Commun.* **50**, 8140–8143 (2014).
38. Cervantes-Navarro, F. *et al*. Stop Rotating! One Substitution Halts the B_{19}^- Motor. *Chem. Commun.* **50**, 10680–10682 (2014).
39. Merino, G. & Heine, T. And Yet It Rotates: The Starter for a Molecular Wankel Motor. *Angew. Chem. Int. Ed.* **51**, 10226–10227 (2012).
40. Heina, T. & Merino, G. What Is the Maximum Coordination Number in a Planar Structure? *Angew. Chem. Int. Ed.* **51**, 4275–4276 (2012).
41. Dong, X. *et al*. Li_2B_{12} and Li_3B_{12}: Pediction of the Smallest Tubular and Cage-like Boron Structures. *Angew. Chem. Int. Ed.* **57**, 4627–4631 (2018).
42. Lau, K. C. & Pandey, R. Highly Conductive Boron Nanotubes: Transport Properties, Work Functions, and Structural Stabilities. *J. Phys. Chem. C* **111**, 2906–2912 (2007).
43. Muya, J. T. *et al*. Jahn-Teller Instability in Cationic Boron and Carbon Buckyballs B_{80}^+ and C_{60}^+: A Comparative Study. *Phys. Chem. Chem. Phys.* **15**, 2892–2835 (2013).
44. Muya, J. T., Gopakumar, G., Nguyen, M. T. & Ceulemans, A. The Leapfrog Principle for Boron Fullerenes: A Theoretical Study of Structure and Stability of B_{112}. *Phys. Chem. Chem. Phys.* **13**, 7524–7533 (2011).
45. Piazzi, Z. A. *et al*. Planar Hexagonal B_{36} as a Potential Basis for Extended Single-Atom Layer Boron Sheets. *Nat. Commun.* **5**, 3113 (2014).
46. Sergeeva, A. P., Zubarev, D. Y., Zhai, H. J., Boldyrev, A. I. & Wang, L. S. A Photoelectron Spectroscopic and Theoretical Study of B_{16}^- and B_{16}^{2-}: An All-Boron Naphthalene. *J. Am. Chem. Soc.* **130**, 7244–7246 (2008).
47. Gerardo, M. G. *et al*. Dynamical Behavior of Borospherene: A Nanobubble. *Sci. Rep.* **5**, 11287 (2015).
48. Popov, I. A., Li, W. L., Piazza, Z. A., Boldyrev, A. I. & Wang, L. S. Complexes between Planar Boron Clusters and Transition Metals: A Photoelectron Spectroscopy and Ab Initio Study of CoB_{12}^- and RhB_{12}^-. *J. Phys. Chem. A* **118**, 8098–8105 (2014).
49. Popov, I. A., Jian, T., Lopez, G. V., Boldyrev, A. I. & Wang, L. S. Cobalt-Centred Boron Molecular Drums with the Highest Coordination Number in the CoB_{16}^- Cluster. *Nat. Commun.* **6**, 8654 (2015).
50. Jian, T. *et al*. Manganese-Centered Tubular Boron Cluster-MnB_{16}^-: A New Class of Transition-Metal Molecules. *J. Chem. Phys.* **114**, 154310 (2016).
51. Jian, T. *et al*. Competition between Drum and Quasi-Planar Structures in RhB_{18}^-: Motifs for Metallo-Boronanotubes and Metallo-Borophenes. *Chem. Sci.* **7**, 7020–7027 (2016).
52. Li, W. L. *et al*. The Planar CoB_{18}^- Cluster as a Motif for Metallo-Borophenes. *Angew. Chem. Int. Ed.* **55**, 7358–7363 (2016).
53. Liang, W. Y., Das, A., Dong, X. & Cui, Z. H. Lithium Doped Tubular Structure in LiB_{20} and LiB_{20}^-: A Viable Global Minimum. *Phys. Chem. Chem. Phys.* **20**, 16202–16208 (2018).
54. Li, W. L. *et al*. Observation of a Metal-Centered B_2-Ta@B_{18}^- Tubular Molecular Rotor and a Perfect Ta@B_{20}^- Boron Drum with the Record Coordination Number of Twenty. *Chem. Commun.* **53**, 1587–1590 (2017).
55. Li, P. F. *et al*. A Detailed Investigation into the Geometric and Electronic Structures of CoB_n^Q ($n = 2-10$, $Q = 0, -1$) Clusters. *New J. Chem.* **41**, 11208–11214 (2017).
56. Bai, H., Chen, Q., Zhai, H. J. & Li, S. D. Endohedral and Exohedral Metalloborospherenes: M@B_{40} (M = Ca, Sr) and M&B_{40} (M = Be, Mg). *Angew. Chem. Int. Ed.* **54**, 941–945 (2015).
57. Liu, C., Si, H., Han, P. & Tang, M. S. Density Functional Theory Study on Structure and Stability of BeB_n^+ Clusters. *Rapid Commun. Mass Spectrom.* **31**, 1437–1444 (2017).
58. Guo, J. C. *et al*. Coaxial Triple-Layered versus Helical $Be_6B_{11}^-$ Clusters: Dual Structural Fluxionality and Multifold Aromaticity. *Angew. Chem. Int. Ed.* **56**, 10174–10177 (2017).
59. Pu, Z. F., Ge, M. F. & Li, Q. S. $MB2^-$ (M = Be, Mg, Ca, Sr, and Ba): Planar Octacoordinate Alkaline Earth Metal Atoms Enclosed by Boron Rings. *Sci. China Chem.* **53**, 1737–1745 (2010).
60. Li, S. D., Miao. C. Q., Guo, J. C. & Ren, G. M. Planar Tetra-, Penta-, Hexa-, Hepta-, and Octacoordinate Silicoons: A Universal Structural Pattern. *J. Am. Chem. Soc*, **126**, 16227–16231 (2004).
61. Sun, W. G., Xia, X. X., Lu, C., Kuang, X. Y. & Hermann, A. Probing the structural and electronic properties of zirconium doped boron clusters: Zr distorted B_{12} ligand framework. *Phys. Chem. Chem. Phys.* **20**, 23740 (2018).
62. Sun, W. G. *et al*. Evolution of the Structural and Electronic Properties of Medium-Sized Sodium Clusters: A Honeycomb-like Na_{20} Cluster. *Inorg. Chem.* **56**, 1241–1248 (2017).
63. Chen, B. L. *et al*. Insights into the effects produced by doping of medium-sized boron clusters with ruthenium. *Phys. Chem. Chem. Phys.* **20**, 30376–30383 (2018).
64. Wang, H. *et al*. CALYPSO Structure Prediction Method and Its Wide Application. *Comput. Mater. Sci.* **112**, 406−415 (2016).

65. Lv, J., Wang, Y. C., Zhu, L. & Ma, Y. M. Particle-Swarm Structure Prediction on Clusters. *J. Chem. Phys.* **137**, 084104 (2012).
66. Wang, Y. C., Lv, J., Zhu, L. & Ma, Y. M. Crystal Structure Prediction via Particle-Swarm Optimization. *Phys. Rev. B* **82**, 094116 (2010).
67. Lu, S. H., Wang, Y. C., Liu, H. Y., Miao, M. S. & Ma, Y. M. Self-Assembled Ultrathin Nanotubes on Diamond (100) Surface. *Nat. Commun.* **5**, 3666 (2014).
68. Wang, H., Tse, J. S., Tanaka, K., Litaka, T. & Ma, Y. M. Superconductive Sodalite-like Clathrate Calcium Hydride at High Pressures. *Proc. Natl. Acad. Sci. USA* **24**, 6463−6466 (2012).
69. Li, Y. W., Hao, J., Liu, H. Y., Li, Y. L. & Ma, Y. M. The Metallization and Superconductivity of Dense Hydrogen Sulfide. *J. Chem. Phys.* **140**, 174712 (2014).
70. Adamo, C. & Barone, V. Toward Reliable Density Functional Methods without Adjustable Parameters: The PBE0 Model. *J. Chem. Phys.* **110**, 6158−6170 (1999).
71. Krishnan, R., Binkley, J. S., Seeger, R. & Pople, J. A. Self-Consistent Molecular Orbital Methods. XX. A Basis Set for Correlated Wave Functions. *J. Chem. Phys.* **72**, 650−654 (1980).
72. Frisch, M. J. *et al*. Gaussian 09 (Revision C.0), Gaussian, Inc., Wallingford, CT, (2009).
73. Casida, M. E., Jamorski, C., Casida, K. C. & Salahub, D. R. Molecular Excitation Energies to High-Lying Bound States from Time-Dependent Density-Functional Response Theory: Characterization and Correction of the Time-Dependent Local Density Approximation Ionization Threshold. *J. Chem. Phys.* **108**, 4439–4449 (1998).
74. Zubarev, D. Y. & Boldyrev, A. I. Developing Paradigms of Chemical Bonding: Adaptive Natural Density Partitioning. *Phys. Chem. Chem. Phys.* **10**, 5207–5217 (2008).
75. Lu, T. & Chen, F. W. Multiwfn: A multifunctional wavefunction analyzer. *Comput. Phys. Commun.* **33**, 580−592 (2012).

Acknowledgements

This work was supported by the National Natural Science Foundation of China (Nos. 11574220 and 11874043) and the Program for Science & Technology Innovation Talents in Universities of Henan Province (No. 15HASTIT020).

Author Contributions

X.Y.K. and C.L. conceived the idea. D.L.K., W.G.S. and C.L. performed the calculations. D.L.K., W.G.S., H.X.S., B.L.C., X.X.X. and G.M. wrote the manuscript. All authors reviewed the manuscript.

Additional Information

Supplementary information accompanies this paper at https://doi.org/10.1038/s41598-019-50905-7.

Competing Interests: The authors declare no competing interests.

Publisher's note Springer Nature remains neutral with regard to jurisdictional claims in published maps and institutional affiliations.